Journal of Materials Chemistry C

Accepted Manuscript

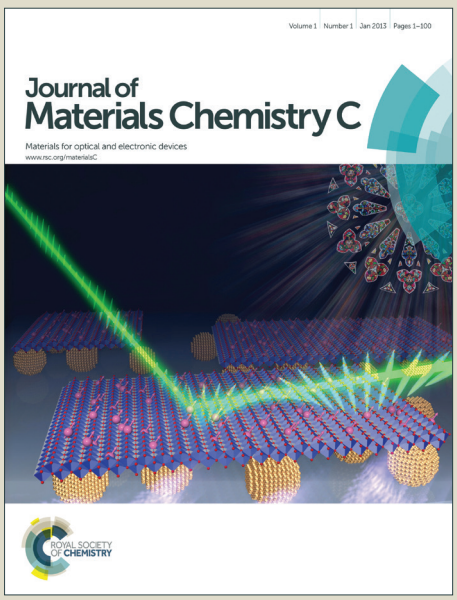

ROYAL SOCIETY OF CHEMISTRY

www.rsc.org/materialsC

Cite this: DOI: 10.1039/c0xx00000x

www.rsc.org/xxxxxx

ARTICLE TYPE

Triisopropylsilylethynyl substituted benzodithiophene copolymers: synthesis, properties and photovoltaic characterization

Enwei Zhu,[a,‡] Guoping Luo,[b,‡] Yun Liu,[a] Jiangsheng Yu,[a] Fujun Zhang,[c] Guangbo Che,[d] Hongbin Wu,*[,b] Weihua Tang*[,a]

Received (in XXX, XXX) Xth XXXXXXXXX 20XX, Accepted Xth XXXXXXXXX 20XX
DOI: 10.1039/b000000x

We demonstrated herein the facile synthesis of triisopropylsilylethynyl (TIPS) functionalized benzo[1,2-b:4,5-b']dithiophene (BDT). Three new TIPSBDT-based donor-acceptor alternating copolymers were further developed by Pd-catalyzed Stille coupling. The effect of accepting unit structure on the optical, electrochemical and energy levels of the polymer was studied. The positive impact of PFN layer, high-boiling solvents processing, polar solvent treatment and solvent annealing on the performance of polymer:$PC_{71}BM$ bulk heterojuction solar cells was revealed. The best devices delivered a power conversion efficiency of 5.46% when blend films processed using o-dichlorobenzene with 3 vol% DIO and treated with the optimization of THF annealing and insertion of PFN layer. The device performance was correlated with the morphology evolution of blend films processed with solvent choice, methanol treatment and THF annealing.

1 Introduction

In the past decades, polymer solar cells (PSCs) have attracted great interest as a promising next-generation green technology in comparison of inorganic silicon-based cells due to their potential advantages of cost-effective, lightweight, and large-scale roll-to-roll production.[1-5] Great progress has been made for PSCs with bulk heterojunction (BHJ) structures, where a polymer/fullerene blend with bicontinuous interpenetrating networks acts as active layer. Tremendous efforts in developing new materials, optimizing film morphology and designing new device architectures have pushed the power conversion efficiency (PCE) of the PSCs.[6-8] Excitingly, the state-of-the-art PCEs have been over 8%, with a champion record of 10.6%.[9-12] Although both the innovation of the material and the optimization of the device structure have led to fairly desirable results, further PSCs commercial application is challenging before the solution of some key issues, such as dependable encapsulation technology to secure long-life working devices and robust large-area processing for device making.[2,9] It is still necessary to find ideal conjugated polymers combining high PCEs with convenient processability in order to meet the requirements of commercialization of PSCs.

Currently, most research is focused on the development of low bandgap polymers with strong and broad absorption, low-lying highest occupied molecular orbital (HOMO) energy levels and high charge mobility. Among various successful polymers utilized for high-efficient solar cells, donor-acceptor (D-A) alternating structure taking advantage of the intramolecular charge transfer (ICT) is one of the most effective approaches to achieve low bandgap polymers.[13-20] To date, benzo[1,2-b:4,5-b']dithiophene (BDT) has been proven to be one of the most successful D units for high-efficient PSC materials.[21-27] Featuring good planarity with two fused thiophene units, BDT allows feasible substitutions on benzene core to fine-tune the energy levels of the resulted derivatives.[28] Triisopropylsilylethynyl functionalized BDT (TIPSBDT) was firstly developed by Li et al, whose low bandgap copolymer delivered a PCE of 4.33% by blending with $PC_{71}BM$.[29] TIPSBDT-quinoxaline alternating polymer contributed a PCE of 2-6%.[30] All these reports inspired us to employ TIPSBDT for constructing new efficient photovoltaic polymers with deep HOMO energy levels. The incorporation of bulky TIPS groups on BDT cores can not only improve the solubility and oxidative stability of the polymers but also promote the π-orbital overlap for higher charge transport. The ethynylene group as an important π-electron linker extended the conjugated system between backbone and silicon atom to facilitate high charge transfer along the side chains. In addition, the D-A copolymers incorporating electron-deficient moieties such as thiazolo[5,4-d]thiazole (TTz)[20,31], or dithienylbenzo[c][1,2,5]oxadiazole (DTBO)[22] units also demonstrated good potential for high-performance PSCs.

From the view of designing new polymers to achieve high-performance PSCs, we are intrigued to know how the alternating of electron-deficient units including TTz, DTBO and thiadiazolo[3,4-g]quinoxaline (DTQx)[32] with TIPSBDT unit can tune the bandgap, absorption and photovoltaic properties of the resulted polymers. On the other hand, the correlation study between device processing strategies and morphology of polymer/fullerene blend in BHJ cells is the key consideration in the pursuit of high-performance PSCs. The device performance can be significantly improved by optimizing the morphology in active layer with insertion of alcohol/water-soluble conjugated

polymer named poly [(9,9-bis(3'-(N,N-dimethylamino) propyl)-2,7-fluorene)-alt-2,7-(9,9-dioctylfluorene)] (PFN) layer,[24,25] use of processing additives,[16,26,27] solvent annealing,[33,34] and polar solvent treatment.[14,22] For example, a PCE of 8.4% was achieved for PBDT-DTNT:$PC_{71}BM$ based devices by inserting a PFN interlayer to optimize the interface between photoactive layer with electrode.[24] Ge et al. reported the hitherto highest PCE of 7% for furan-containing PSCs through simply solvent treatment before deposition of the metal electrodes.[22]

In this study, we demonstrated the facile synthesis of TIPSBDT via Sonogashira coupling between trimisopropylsilyl acetylene and BDT triflate. Three BDT based new copolymers (i.e., PTIPSBDT-TTz, PTIPSBDT-BO and PTIPSBDT-DTQx) were further developed. We investigated the synthesis, thermal stability, optical and electrochemical properties, and pristine photovoltaic characteristics of the resulting polymers. Further device optimization was conducted by insertion of PFN layer, screening of solvent and additive, solvent annealing and polar solvent treatment. Encouragingly, PTIPSBDT-TTz:$PC_{71}BM$ devices exhibited a great enhancement in PCE, with the highest efficiency of 5.46% obtained. The enhanced device performance was further correlated with morphology study.

2 Results and discussion

2.1 Synthesis and characterization

The synthetic routes for donating monomer TIPSBDT as well as polymers are outlined in Scheme 1. The TIPSBDT monomer was synthesized in 90% yield using Sonogashira coupling between trimisopropylsilyl acetylene and BDT triflate (1). BDT triflate was developed as a versatile coupling reagent for various Pd-catalyzed cross-coupling for direct access of 4,8-bifunctionalized BDTs.[28] With tin reagent of TIPSBDT at hand, its polycondensation with dibrominated electron-accepting monomers was conducted via Pd-catalyzed Stille coupling to afford three new TIPSBDT-based copolymers. After Soxhlet extraction with methanol, hexane and chloroform in sequence, the pure polymers were obtained with a yield of 82% for PTIPSBDT-TTz, 75% for PTIPSBDT-DTBO, 80% for PTIPSBDT-TPD and 88% for PTIPSBDT-DTQx.

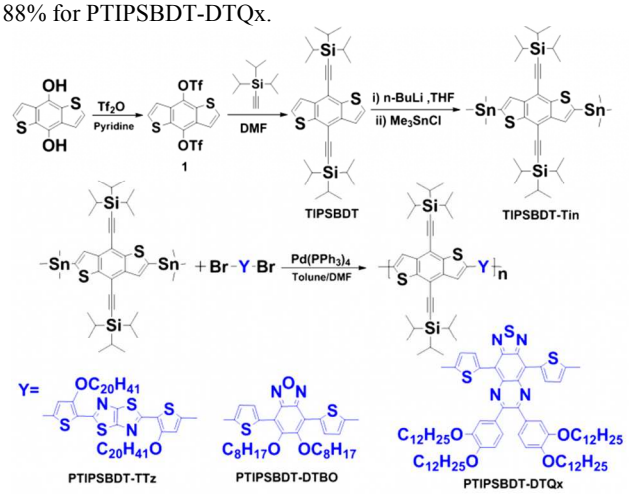

Scheme 1 Synthetic route to TIPSBDT-based donor-acceptor copolymers.

All polymers exhibit good solubility in common organic solvents such as THF, chloroform (CF), chlorobenzene (CB) and toluene. The molecular weight and polydispersity index (PDI) were measured by GPC analysis. Polymers exhibited a number-average molecular weight (M_n) of 10-15 kDa, with a corresponding PDI ranging from 1.38 to 1.48. The thermal stability of three polymers was investigated with TGA analysis, with the TGA traces plotted in Figure S11. A degradation temperature (T_d, corresponding to 5% weight loss) of polymer was found to be 310°C for PTIPSBDT-TTz, 380°C for PTIPSBDT-BO, and 360°C for PTIPSBDT-DTQx. These high T_d values indicate the good thermal stability of the polymers, which are beneficial for their application in optoelectronic devices.[6]

2.2 Optical Properties

The UV-vis absorption spectra of three polymers in dilute CF solutions (~1×10^{-5} M) and in thin films are shown in Figure 1, with the corresponding absorption data summarized in Table 1. As shown, all polymers exhibit two distinct absorption bands. The absorption at ultraviolet region can be ascribed to the π-π* transition of their main chain units and the absorption at the visible region can be attributed to the CT absorption of polymer main chains.[6] PTIPSBDT-TTz solution showed long absorption band in 600-680 nm region with an absorption maximum (λ_{max}) at 616 nm. Compared with its solution, PTIPSBDT-TTz film exhibited 12 nm red-shifted λ_{max} and 70 nm red-shifted absorption edge (λ_{onset}), indicating the strong intermolecular interaction and aggregation occurring in the solid-state of polymer. PTIPSBDT-DTBO film exhibited broad absorption spectra with a λ_{max} at 619 nm and absorption shoulder in the range of 500-700 nm, which was ~20 nm red-shifted in comparison to its dilute solution. This may be explained with the effective intermolecular π-π packing interactions in its solid state.

PTIPSBDT-DTQx films, however, exhibited a remarkably red-shifted absorption (~ 80 nm) with a λ_{onset} up to 950 nm in comparison to its dilute solution, suggesting the strongest ICT absorption along polymer backbones caused by the strong electron-withdrawing properties of DTQx units as well as the large conjugated fused-ring system. Meanwhile, the long-wavelength band of PTIPSBDT-DTQx is almost completely located in the near-infrared area and determines the ability of this material to absorb photons of the solar spectrum with the lowest energy.[32,35]

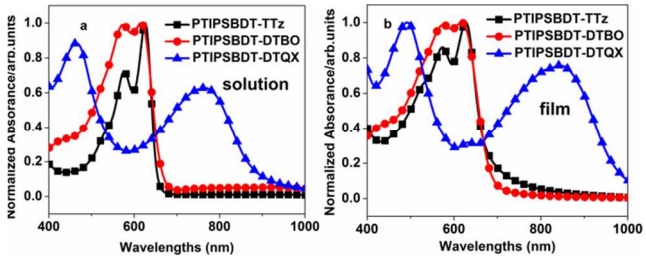

Fig.1 UV-vis absorption spectra of (a) polymer solutions in diluted $CHCl_3$ and (b) polymer films drop-cast on quartz.

The optical bandgap (E_g^{opt}) of polymers can be estimated with the λ_{onset} values of polymer films according to the empirical equation $E_g^{opt} = 1240/\lambda_{onset}$. The E_g^{opt} of polymers were thus calculated to be 1.69, 1.76 and 1.31 eV for PTIPSBDT-TTz, PTIPSBDT-DTBO and PTIPSBDT-DTQx, respectively. The small bandgaps (<2.0 eV) of three polymers were successfully achieved by the strong ICT effect between the donating and the

accepting units. Obviously, the bandgaps of TIPSBDT polymers can be easily tuned by adjusting the electron withdrawing units.

Table 1 Optical and electrochemical properties of polymers

Polymer	λ_{max}[a] (nm)	λ_{onset}[a] (nm)	λ_{max}[b] (nm)	λ_{onset}[b] (nm)	E_g^{opt} (eV)[c]	HOMO (eV)[d]	LUMO (eV)[e]
PTIPSBDT-TTz	616	665	628	734	1.69	-5.53	-3.84
PTIPSBDT-DTBO	615	680	619	702	1.76	-5.50	-3.74
PTIPSBDT-DTQx	762	907	843	950	1.31	-5.40	-4.09

[a]UV-vis absorption in dilute $CHCl_3$ solution, [b]UV-vis absorption in thin films, [c]$E_g^{opt} = 1240/\lambda_{onset}$, [d]HOMO = -e($E_{onset}^{ox}$ + 4.4) (eV), [e]LUMO = HOMO + E_g^{opt}

2.3 Electrochemical properties

The highest occupied molecular orbital (HOMO) and the lowest unoccupied molecular orbital (LUMO) energy levels of the conjugated polymers can be determined with CV measurements. The CV traces of polymers films on Pt electrode are shown in Figure 2a, with the potential of ferrocene 0.40 V vs SCE used as internal standard. On the basis of 4.8 eV below vacuum for the energy level of Fc/Fc+, the HOMO level of the polymers is calculated from the onset oxidation potentials (E_{ox}^{onset}) with equation: HOMO = -e(E_{ox}^{onset}+4.4) (eV). The E_{ox}^{onset} of PTIPSBDT-TTz, PTIPSBDT-DTBO, and PTIPSBDT-DTQx was observed to be 1.09, 1.06 and 1.00 eV, respectively. Accordingly, the HOMO energy level of PTIPSBDT-TTz, PTIPSBDT-DTBO, PTIPSBDT-TPD and PTIPSBDT-DTQx is determined as -5.53, -5.50 and -5.40 eV, respectively.

Since only oxidation peaks of polymer films were obtained, the LUMO levels of polymers were calculated using HOMO and E_g^{opt} according to the equation: LUMO = HOMO+E_g^{opt} (eV). The LUMO level of PTIPSBDT-TTz, PTIPSBDT-DTBO and PTIPSBDT-DTQx was thus calculated to be -3.84, -3.74 and -4.09 eV, respectively. The HOMO-LUMO energy diagrams of the polymers and $PC_{71}BM$ are shown in Figure 2b. Apparently, all these polymers exhibited deep HOMO levels close to the ideal value (ca. -5.4 eV)[36] for high-efficiency PSCs, indicating that these polymers when used as donors for BHJ cells could generate desirable V_{oc} and maintain good chemical stability at ambient conditions. Three polymers exhibited almost identical HOMO energy levels, due to the presence of the same BDT donating moiety. Importantly, PTIPSBDT-TTz and PTIPSBDT-DTBO also show good LUMO energy levels, which are beneficial for the electrons transfer from polymer donors to $PC_{71}BM$, because the efficient exciton separation is provided that the energy offset between the polymer and fullerene (LUMO) is at least 0.3 eV. These results further demonstrated the ability of tuning the energy levels by changing accepting units for D-A polymers.

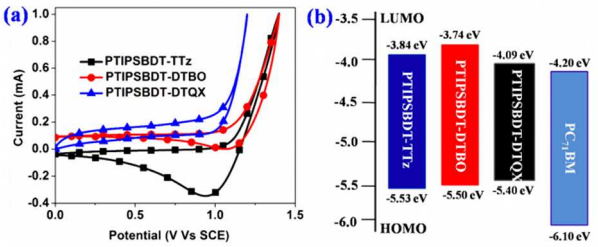

Fig. 2 (a) Oxidation scans of cyclic voltammograms of polymer thin films in 0.1 M Bu_4NPF_6 acetonitrile solutions at 50 mV/s scan rate, (b) the HOMO-LUMO energy levels of the copolymers.

2.4 Photovoltaic properties

To evaluate the potential of the polymers in PSCs application, BHJ cells were fabricated with the device configuration of ITO/PEDOT:PSS(40nm)/Active layer (~90 nm)/with or w/o PFN (5 nm)/Al (100 nm). Firstly, the PSC devices were fabricated by spin-coating the active layers from CF solutions. Different weight ratios of copolymer donor to $PC_{71}BM$ (1:1 and 1:2) were studied. We found that the optimal D:A ratio was 1:2 for PTIPSBDT-TTz while 1:1 for other three polymers. The *J-V* curves of the PSC devices under solar illumination (AM1.5G, 100 mW cm^{-2}) and under dark are shown in Figure S12, with the deduced parameters summarized in Table S1. PTIPSBDT-TTz, PTIPSBDT-DTBO and PTIPSBDT-DTQx based PSCs showed a relatively high V_{oc} of 0.79, 0.80, and 0.73 V, respectively. The discrepancies may be explained with the deeper low-lying HOMO energy levels of the first three polymers (Figure 2b). Among of them, PTIPSBDT-DTQx based cells exhibited quite low J_{sc} and FF, resulting in a PCE lower than 0.15%. This may be explained with its deep-lying LUMO level, close to that of $PC_{71}BM$, which cannot ensure sufficient driving force to promote the charge transfer from the polymer donor to fullerene acceptor.[5]

As known, PFN could lead to better interfacial contacts through decreasing the series resistance, benefiting for the enhanced electron collection of the cathode as well as decreased possibility of hole-electron recombination in the active layer.[9,24] The effect of PFN interlayer on the device performance was studied for our PSCs. As expected, inserting the cathode interfacial layer PFN had much improvement on the performance of devices (Table S1). For instance, for PTIPSBDT-TTz:$PC_{71}BM$ (1:2) device, the device with Al cathode displayed an initial PCE of 0.89%, while a high PCE of 1% was obtained for device when PFN was introduced as the cathode interlayer. The improved PCE was attributed mainly to the obvious enhancement in V_{oc} and FF. This enhancement was also observed for PTIPSBDT-DTBO and PTIPSBDT-DTQx based devices. Particularly, PTIPSBDT-DTBO:$PC_{71}BM$ (1:1) device exhibited a remarkable enhancement of V_{oc} from 0.8 V to 0.96 V. The observed enhancement of V_{oc} could be revealed by the *J-V* characteristics of the devices in the dark (Figure S12).

The low device performance for devices processed from CF solutions may indicate the poor solubility of polymer:$P_{71}CBM$ in CF. At present, the widely processing solvents for spin-coating are high boiling-point solvents of CB[8,17] and o-DCB[11,16] due to their good solvation properties and low evaporation rates, which allows the blend of polymer/fullerene to organize into optimal microstructure. On the other hand, the DIO as solvent additive is often used to be the cosolvent due to its prolonged evaporation time and preferential solubility for $PC_{71}BM$, leading to the formation of aggregation of the conjugated polymer and increment of the degree of phase separation. Based on this strategy, we tried to use the mixed solvent of CB or o-DCB with 3 vol% DIO as an additive for processing the active layer to optimize the Photovoltaic Performance.[16,26] Figure 3 show the *J-V* characteristics of polymer/$PC_{71}BM$ devices processed using a mixed solvent of CB or o-DCB with 3 vol% DIO. The effect of insertion of PFN interlayer and methanol treatment of active layer

on device performance was studied for PTIPSBDT-TTz:$PC_{71}BM$ (1:2) and PTIPSBDT-DTBO:$PC_{71}BM$ (1:1) based devices. The photovoltaic parameters of the devices are summarized in Table 2.

Table 2 Comparison of photovoltaic properties of polymer/$PC_{71}BM$ based devices parepared from CB:DIO or o-DCB:DIO (97:3, v/v) with PFN interlayer and methanol treatment

Active layer[a]	D:A (wt%)	Treatment	V_{oc} (V)	J_{sc} (mA/cm^2)	FF (%)	PCE_{max}(%)[f]
PTIPSBDT-TTz: $PC_{71}BM$	1:2	As cast[b]	0.64	9.12	33.8	1.97 (1.86)
		PFN[b,d]	0.76	9.47	37.5	2.70 (2.64)
		Methanol[b,e]	0.77	9.63	41.5	3.08 (2.99)
		As cast[c]	0.77	9.84	43.4	3.29 (2.96)
		PFN[c,d]	0.89	10.5	53.5	4.99 (4.38)
		Methanol[c,e]	0.88	10.4	54.8	5.02 (4.62)
PTIPSBDT-DTBO: $PC_{71}BM$	1:1	As cast[b]	0.71	3.74	30.8	0.82 (0.76)
		PFN[b,d]	0.89	5.76	35.7	1.83 (1.64)
		Methanol[b,e]	0.95	6.51	39.0	2.41 (2.30)
		As cast[c]	0.63	5.24	34.6	1.14 (1.09)
		PFN[c,d]	0.97	6.72	42.4	2.77(2.50)
		Methanol[c,e]	0.95	6.48	41.0	2.52 (2.18)

[a]Cell structure was ITO/PEDOT:PSS(40 nm)/Active layer(~90 nm) /Al(100 nm); [b]The active layers spin-coated from the mixed solvent of CB +3 vol% DIO; [c]The active layers spin-coated from the mixed solvent of o-DCB +3 vol% DIO; [d]The PFN layer was inserted; [e]active layers were treated by methanol; [f]The average PCE was given in parentheses.

The as-cast device structure was ITO/PEDOT:PSS/polymer:$PC_{71}BM$/Al. As shown in Table 2, devices fabricated using CB:DIO or o-DCB:DIO (97:3, v/v) mixture solvent exhibited significantly increased performance in comparison to those using CF. For example, when processed using CB+3% DIO, PTIPSBDT-TTz device obtained an increased PCE from 0.89% to 1.97%, while PTIPSBDT-DTBO devices showed an increased PCE from 0.62% to 0.82%. When processed using o-DCB:DIO (97:3, v/v), the device incorporating PTIPSBDT-TTz, PTIPSBDT-DTBO and $PC_{71}BM$ achieved further improved from 1.97% to 3.29% and from 0.82% to 1.14%, respectively. The enhancement in PCE for devices processed from different solvents may be explained with the solubility of $PC_{71}BM$ and the morphology of active layer, where smaller domain sizes for $PC_{71}BM$ were observed. Similar enhancement of PCE for device processed using CB instead of CF was also found for the TIPSBDT polymer based devices.[8,29]

Compared with the as-cast devices, devices with PFN interfacial layer showed simultaneous enhancement in all device parameters, resulting in dramatically increased PCE values. For instance, PTIPSBDT-TTz: $PC_{71}BM$ (1:2) device fabricated from CB-DIO (3%) solvent gave a much improved PCE from 1.97% to 2.70%, with V_{oc} increased from 0.64 to 0.77 V, J_{sc} from 9.12 to 9.63 mA/cm^2 and FF from 33.8% to 41.5%. The PTIPSBDT-TTz-based device fabricated from o-DCB-DIO (3%) obtained an increased PCE from 2.70% to 4.99% with a largely increased V_{oc} from 0.76 V to 0.89 V and FF from 37.5% to 53.5% (Figure 3c, Table 2). For the PTIPSBDT-DTBO-based devices, an improved PCE of 1.83% was achieved with the spin-coating solvent of 97% CB/3% DIO compared to that of CF. With o-DCB:DIO (97:3, v/v) as spin-coating solvent, the corresponding devices showed further increased PCE from 1.83% to 2.77% accompanied with simultaneously improvement of V_{oc} from 0.89 V to 0.97 V and FF from 37.5% to 42.4%. A noteworthy fact is that the devices with PFN layer show a dramatically improvement in the V_{oc} relative to those of the analogues without PFN layer. This result agrees well with the results reported by Wu et al. that the PFN interlayer led to simultaneous enhancement of all parameters in the based PTB7:$PC_{71}BM$ device.[9]

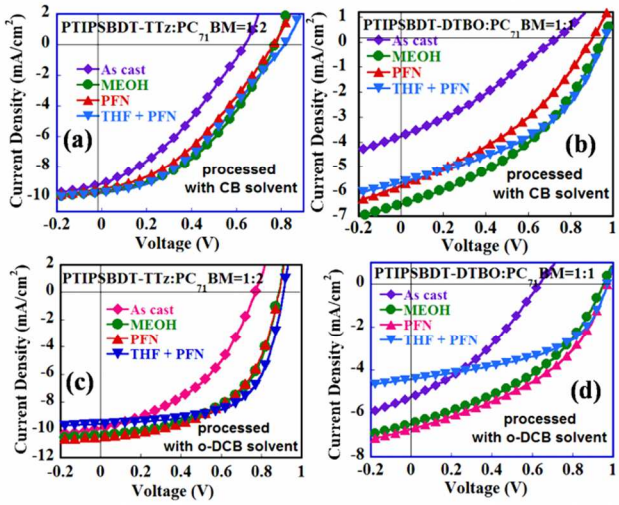

Fig. 3 (a) *J-V* characteristics of photovoltaic devices processed using CB:DIO (97:3 v/v) solvent based on (a) PTIPSBDT/$PC_{71}BM$ (1:2, w/w), and (b) PTIPSBDT-DTBO/$PC_{71}BM$ (1:1, w/w) with different fabricated conditions under illumination of AM1.5G (100 mW/cm^2); *J-V* characteristics of photovoltaic devices processed using o-DCB:DIO (97:3 v/v) solvent based on (c) PTIPSBDT/$PC_{71}BM$ (1:2, w/w), and (d) PTIPSBDT-DTBO/$PC_{71}BM$ (1:1, w/w) with different fabricated conditions under illumination of AM1.5G (100 mW/cm^2).

The active layer through simple polar solvent treatment was reported to form fiberlike interpenetrating morphologies benefiting from the increased hole mobilities as well as more-balanced charge transport, which resulted in the simultaneous enhancement of device parameters of PSCs.[14,22] However, much less attention has been paid to their beneficial influence on the performance of PSCs. We tried to employ methanol as polar solvent to optimize the performance of PSCs. Inspiringly, after methanol exposure, the PSCs achieved dramatically improved performance. From Table 3, one can see that the influence of methanol treatment depends on the processing solvent. The PTIPSBDT-TTz devices spin-coated with CB-DIO (3%) solvent exhibited a much increased PCE of 3.08%, with J_{sc} increased from 5.76 to 9.63 mA/cm^2, V_{oc} from 0.64 to 0.76 V and FF from 33.8% to 37.5%. On the basis of the same structure of ITO/PEDOT:PSS(40 nm)/Active layer(~90 nm) /Al(100 nm), the PCE of devices based on PTIPSBDT-TTz with o-DCB:DIO (3%) as spin-coating solvent was further significantly improved to 5.02% with a J_{sc} of 10.4 mA/cm^2, a V_{oc} of 0.88 V, and an FF of 54.8%. The trend of the device based on PTIPSBDT-DTBO with methanol treatment was similar to that of the above-mentioned PTIPSBDT-TTz. The PTIPSBDT-DTBO devices with CB:DIO (3%) mixed solvent also showed a significantly increased PCE from 0.82% to 2.41% after the exposure of active layers to methanol. The further increased PCE of 2.52% was achieved in the PSCs based on PTIPSBDT-DTBO with o-DCB:DIO (3%) solvent.

Solvent annealing of active layer is well recognized to enhance its light absorption and the hole mobility by inducing the self-

organization of polymers, resulting in improved efficiency for PSCs.[33,34] THF was herein chosen as the low boiling-point solvent to study the effect of solvent annealing on device performance. The *J-V* characteristics of ITO/PEDOT:PSS/polymer:$PC_{71}BM$/PFN/Al devices with or w/o THF annealing are shown in Figure 3a-d and device data were summarized in Table 4. With "solvent annealing", PTIPSBDT-TTz:$PC_{71}BM$ (1:2) device with CB:DIO (97:3,v/v) as the spin-coating solvent achieved an increased PCE of 2.96% (by 9.6%), with dramatic increase in V_{oc} from 0.76 to 0.81 V and slight increase of J_{sc} from 9.47 to 9.75 mA/cm^2 but unchanged FF. When replacing CB with o-DCB as parent solvent, the PTIPSBDT-TTz-based device gave the highest PCE of 5.46% with a J_{sc} of 9.57 mA/cm^2, a V_{oc} of 0.91 V, and an FF of 62.7%. It was identically observed that The PTIPSBDT-DTBO:$PC_{71}BM$ (1:1,w/w) device prepared from CB:DIO (97:3, v/v) solvent also presented an increment (by 25%) in PCE from 1.83 to 2.29%, with FF increased from 35.7 to 42.8% and V_{oc} increased from 0.89 to 0.95 V after solvent annealing. Incorporating 3% DIO into the spin-coating solvent of o-DCB, however, the PTIPSBDT-DTBO device showed a declined PCE of 2.10% attributed to the reduced J_{sc}. These results indicate that the solvent annealing is effective to improve device performance, which are attributed to the healing of the disruption in the ordering of polymer donors induced by incorporating $PC_{71}BM$ molecules in the blend system.[34]

Table 4 Comparison of the photovoltaic properties of polymer/$PC_{71}BM$-based devices with or w/o THF annealing

Active layers[a]	D:A (wt%)	Treating time (s)	V_{oc} (V)	J_{sc} (mA/cm^2)	FF (%)	PCE_{max} (%)
PTIPSBDT-TTz:$PC_{71}BM$	1:2	0[b]	0.76	9.47	37.5	2.70 (2.80)
		30[b,d]	0.81	9.75	37.5	2.96 (2.61)
		0[c]	0.89	10.5	53.5	4.99 (4.38)
		30[c,d]	0.91	9.57 (10.1)[e]	62.7	5.46 (5.34)
PTIPSBDT-DTBO:$PC_{71}BM$	1:1	0[b]	0.89	5.76	35.7	1.83 (1.64)
		30[b,d]	0.95	5.63	42.8	2.29 (2.20)
		0[c]	0.97	6.72	42.4	2.77 (2.50)
		30[c,d]	0.97	4.42	50.0	2.15 (2.10)

[a]Cell structure was ITO/PEDOT:PSS(40 nm)/Active layer(~90 nm)/THF solvent treatment 30 s /PFN (5 nm)/Al(80 nm);. [b]The active layers spin-coated from the mixed solvent of CB +3 vol% DIO; [c]The active layers spin-coated from the mixed solvent of o-DCB +3 vol% DIO; [d]The active layer was THF annealing for 30s; [e]The value in the parentheses is integrated current calculated from IPCE spectrum.

2.5 IPCE

The incident photon-to-current efficiency (IPCE) of the solar cells was measured under the illumination of monochromatic light. Figure 4 shows the IPCE curves of the best performance PTIPSBDT-TTz and PTIPSBDT-DTBO devices, which are also used to verify the measured J_{sc} values. PTIPSBDT-TTz:$PC_{71}BM$(1:2)/PFN/Al devices processed using CB+3 vol% DIO exhibited a high photo-to-current response in the region of 400~700 nm. With a maximum IPCE of 55.5% peaking at 560 nm, the PTIPSBDT-TTz devices exhibit a broad photo-response of over 50% in the range of 450-650 nm, suggesting a highly efficient photo conversion process and balanced charge transport in the devices. Although PTIPSBDT-DTBO:$PC_{71}BM$ devices presented lower IPCE values than PTIPSBDT-TTz devices, broad response ranges covering 380-660 nm were obtained and a relatively high IPCE value above 35% in the region of 400-650 nm. The IPCE values of PTIPSBDT-DTBO-based devices were observed to be lower than those of PTIPSBDT-TTz devices, which agreed with its lower J_{sc} values than PTIPSBDT-TTz based devices.[11] The J_{sc} of PTIPSBDT-TTz calculated from the integral of IPCE curves is consistent with the J_{sc} value obtained from the *J-V* curves in the Figure 3c.

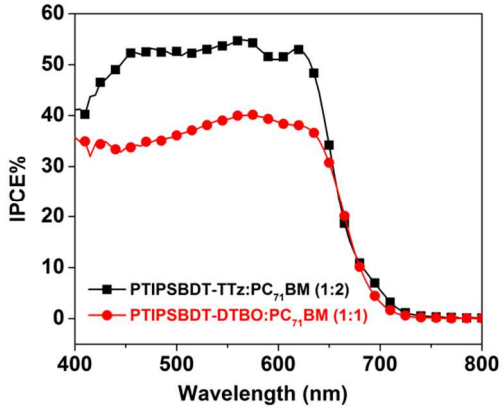

Fig. 4 IPCE spectrum of best performing polymer:$PC_{71}BM$ solar cells under illumination of AM 1.5G (100 mW/cm^2).

2.6 Morphology

In order to gain more insight for the observed difference in device performance, tapping-mode atomic force microscopy (AFM) was employed to characterize the surface morphological properties of PTIPSBDT-TTz/$PC_{71}BM$ and PTIPSBDT-DTBO/$PC_{71}BM$ blend films prepared with different D/A weight ratios, processing solvents, methanol solvent exposure and THF annealing. When increasing the weight ratio of polymer/$PC_{71}BM$ from 1:1 to 1:2, the domains size of $PC_{71}BM$ increased for all active layers processed using CF (Figure 5a-b and 5c-d). The relatively large (100-300 nm) globular clusters assigned to $PC_{71}BM$ domains were observed in PTIPSBDT-TTz, implying poor uniform distribution of PTIPSBDT-TTz and $PC_{71}BM$. However, the phase images of PTIPSBDT-DTBO:$PC_{71}BM$ films showed obscure interfaces between two phases with uniform domain sizes for the dispersed $PC_{71}BM$ phase. The polymer:$PC_{71}BM$ blend films show a root mean square roughness (RMS) of 12.142 and 3.469 nm in the topography for PTIPSBDT-TTz and PTIPSBDT-DTBO, respectively. When spin-coating the active layers from CB solution with 3% DIO additive, the active layers presented much finer and more uniform morphology, as shown as the right column in Figure 5c and 5f. The big difference in film morphology indicates that the polymer:$PC_{71}BM$ blend had better solubility in CB solution with 3% DIO than CF. Nanoscale phase separation was observed in all active layers with rather small RMS (3.4~4.1 nm). Especially, PTIPSBDT-TTz/$PC_{71}BM$ (1:2) films exhibited good phase separation and dramatically decreased RMS (4.123 nm). Under the same condition, PTIPSBDT-DTBO:$PC_{71}BM$(1:1) blend films exhibited much improved miscibility between PTIPSBDT-DTBO and $PC_{71}BM$, leading to the formation of closely interpenetrating networking of fibrous phases. The film showed increased Rms from 2.551 to 3.420 nm when shifting solvent from CF to CB+

3% DIO. The improved morphology PTIPSBDT-DTBO:$PC_{71}BM$ (1:1) film are in good agreement with the enhanced J_{sc} observed for the devices.[16] As shown in Figure 5g and 5i, different phase images occurred when the blend films of the active layers were processed with the o-DCB solution with 3% DIO in comparison whit that of CB solution with 3% DIO. For example, the blend film incorporating PTIPSBDT-TTz with $PC_{71}BM$ showed continuous fibril domains phase with similar RMS of 4.290 nm, which is favorable for the charge transportation, affording significantly improved FF.[9,33] The PTIPSBDT-DTBO-based blend film, however, showed fibril domains phase accompanied with appearance of the dark regions owning to the aggregated $PC_{71}BM$.

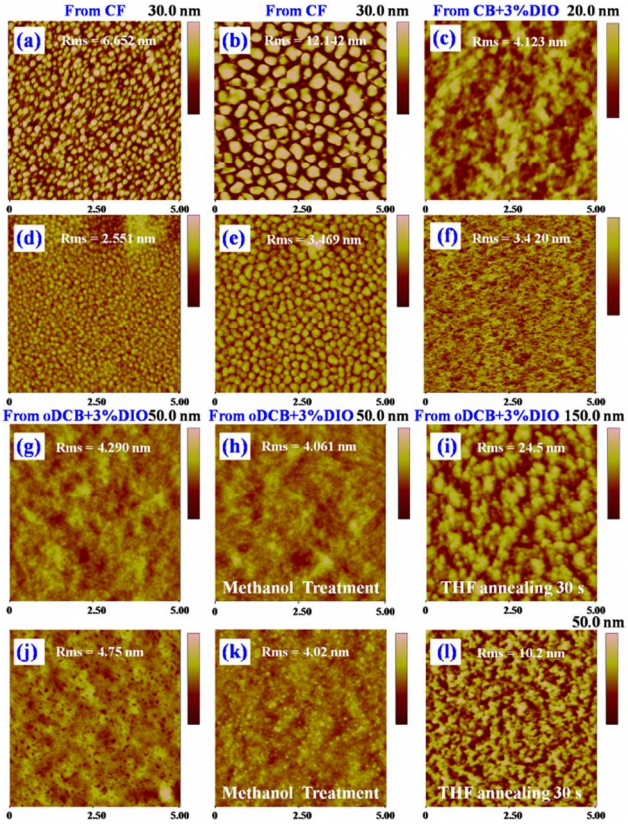

Fig. 5 AFM topographic images (5×5 μm) for thin films of (a) PTIPSBDT-TTz:$PC_{71}BM$ (1:1, w/w), (b) PTIPSBDT-TTz:$PC_{71}BM$ (1:2, w/w), (c) PTIPSBDT-TTz/$PC_{71}BM$ (1:2) using CB+3% DIO, (d) PTIPSBDT-DTBO:$PC_{71}BM$ (1:1, w/w), (e) PTIPSBDT-DTBO:$PC_{71}BM$ (1:2, w/w), (f) PTIPSBDT-DTBO/$PC_{71}BM$ (1:1) using CB+3% DIO, (g) PTIPSBDT-TTz/$PC_{71}BM$ (1:2) using o-DCB+3% DIO, (h) PTIPSBDT-TTz/$PC_{71}BM$ (1:2) using o-DCB+3% DIO with methanol treatment, (i) PTIPSBDT-TTz/$PC_{71}BM$ (1:2) using o-DCB+3% DIO with THF annealing, (j) PTIPSBDT-DTBO/$PC_{71}BM$ (1:1) using o-DCB+3% DIO, (k) PTIPSBDT-DTBO/$PC_{71}BM$ (1:1) using o-DCB+3% DIO with methanol treatment, (i) PTIPSBDT-DTBO/$PC_{71}BM$ (1:1) using o-DCB+3% DIO with THF annealing.

Subsequently, In the case of PTIPSBDT-TTz:$PC_{71}BM$ blends, it could be observed that the blend film with solvent exposure exhibited relatively much smaller fibril domains phase between the polymer and $PC_{71}BM$ with a reduced RMS of 4.06 nm (Figure 5h). This observation indicates that the surface composition distribution of the blend film may be changed by methanol treatment, which was responsible for the dramatically enhancement of the PCE. For the methanol-treated films incorporating PTIPSBDT-DTBO with $PC_{71}BM$, the dark morphologies of Figure 5j were disappeared and bright regions occurred in Figure 5k. For the PTIPSBDT-TTz/$PC_{71}BM$ (1:2) blend film, a more uniform distribution of PTIPSBDT-TTz and $PC_{71}BM$ and the formation of fiberlike interpenetrating morphologies at the length scale of ~20 nm with RMS of 24.5 nm after THF annealing were observed, which was evidenced from Figure 5i. Obviously, the self-organization of the active layer was induced and continuous interpenetrating network films were produced after THF annealing, which is essential for the exciton separation and charge transport. This is consistent with its highest efficiency and FF. Similarly, dramatic changes in the film morphology of the blend comprising PTIPSBDT-DTBO and $PC_{71}BM$ (Figure 5l) were observed compared to that of devices without THF annealing. The self-organization of the active layer formed with RMS of 10.2 nm in the phase images and the appropriate phase separation was also responsible for the enhancement of FF.

3. Conclusions

We have reported the facile synthesis of TIPSBDT unit via the Sonogashira coupling between trimisopropylsilyl acetylene and BDT triflate. By alternating with different accepting units a series of TIPSBDT-based D-A polymers were further developed. The impact of accepting unit structures on the optical, thermal, electrochemical and photovoltaic properties of the resulted polymers was investigated in details. PTIPSBDT-DTQx exhibited an absorption extending to 1000 nm due to the strong electron-withdrawing property of DTQ_X unit. The ITO/PEDOT:PSS/polymer:$PC_{71}BM$/PFN/Al devices processed using CB solutions with 3 vol% DIO delivered a PCE of 2.70% and 1.83% for PTIPSBDT-TTz and PTIPSBDT-DTBO respectively. Incorporating 3% DIO into the spin-coating o-DCB solutions, the as-prepared device obtained from blends of PTIPSBDT-TTz and PTIPSBDT-DTBO with $PC_{71}BM$ achieved a PCE of 4.99% and 2.77%, respectively. Cheerfully, the device incorporating PTIPSBDT-TTz with $PC_{71}BM$ that was processed involving THF annealing and o-DCB-DIO (3%) exhibited the highest PCE of 5.46% with J_{sc} of 9.57 mA/cm^2, a V_{oc} of 0.91 V, and an FF of 62.7%.In addition, the performance of the device with the structure of ITO/PEDOT:PSS/ PTIPSBDT-TTz:$PC_{71}BM$/Al was found to be further improved from 3.08% to 5.02% with exposure of the active layers to methanol and o-DCB-DIO (3%) instead of CB-DIO (3%) as spin-coating solvent. The morphology studies revealed that polymer:$PC_{71}BM$ had better solubility in CB solution with 3vol% DIO than in CF. Active layers processed from CB+3% DIO exhibited nanoscale phase separation and low surface roughness, which contributed for the efficient charge transfer to achieve high J_{sc} and FF for the devices. For the PTIPSBDT-TTz:$PC_{71}BM$ blend, phase separation in o-DCB-DIO (3%) spin-coated film was much better than that of CB-DIO (3%). The further methanol exposure to the blend film gave rise to the optimized morphology for PTIPSBDT-TTz and PTIPSBDT-DTBO respectively, which was responsible for simultaneous enhancement of V_{oc}, J_{sc}, and FF in PSCs. It is worth noting the films prepared from o-DCB-DIO (3%) exhibited morphologies of obvious self-organization after THF annealing. Especially, the interpenetrating network films

with the length scale of ~20 nm were produced for PTIPSBDT-TTz. This work demonstrates the correlation of the morphology evolution of blend films and photovoltaic properties of the resulted polymers and offers simple and effective methods to improve the efficiency of PSCs by interfacial engineering, solvent choice, polar solvent treatment and solvent annealing.

4. Experimental

4.1. Materials

All starting materials and reagents were purchased from Sigma-Aldrich Chemical Co. and used without further purification. THF was dried over sodium/benzophenone and freshly distilled before use. 4,8-Dihydroxybenzo[1,2-b:4,5-b']dithiophene,[28] TTz,[20] DTBO[22] and DTQx[32] were synthesized according to previously reported procedures. Detailed synthesis and purification procedures for the intermediate compounds and characterization details are given in the Electronic Supplementary Information (ESI).

*4,8-Bis(trifluoromethanesulfonyloxy)-benzo[1,2-b:4,5-b']dithiophene (**1**).*[28] Under N_2 atmosphere, to a suspension of 4,8-dihydroxybenzo[1,2-b:4,5-b']dithiophene (6 g, 27 mmol) and dry pyridine (6.6 mL) in dichloromethane (150 mL) was slowly added with trifluoromethanesulfonic anhydride (13.6 mL, 80 mmol) at 0°C. After the mixture was stirred at 0°C for 12 h, water (100 mL) and hydrochloric acid (100 mL, 1 M) were added. The resulting mixture was extracted with dichloromethane (3×80 mL). The combined organic layers were dried over $MgSO_4$ and concentrated in vaccuo. The residue was purified through column chromatography on silica gel eluted with petroleum ether/ethyl acetate (19:1, v/v) to give the pure *title* compound as a white solid (9 g, 70%). ^{1}H NMR (500 MHz, DMSO-d_6, ppm) δ: 8.22 (d, J = 5.5 Hz, 2H), 7.57 (d, J = 5.5 Hz, 2H).

4,8-Di(triisopropylsilylethynyl)-benzo[1,2-b:4,5-b']dithiophene (TIPSBDT). The bistriflate **1** (3 g, 6.1 mmol), triisopropylsilyl acetylene (3.44 mmol, 15.2 mmol), $Pd(PPh_3)_2Cl_2$ (85.5 mg, 0.06 mmol, 10 mol%) and CuI (45 mg, 0.12 mmol, 20 mol%) were placed in a round-bottomed flask (50 mL) under nitrogen. DMF (7 mL) and diisopropylamine (7 mL) was added via a septum. The mixture was stirred for 12 h at 100°C then poured onto aqueous hydrochloric acid (1 mL, 1 M). The resulting mixture was extracted with dichloromethane (3×10 mL), and the combined organic layer was dried over $MgSO_4$ and concentrated in vaccuo. The residue was purified by column chromatography on silica gel eluted with hexane to give the *title* compound as a yellow solid (3 g, 90%). ^{1}H NMR (500 MHz, DMSO-d_6, ppm) δ: 7.60 (d, J = 5.5 Hz, 2H), 7.55 (d, J = 5.5 Hz, 2H), 1.20 (m, 42H).

2,6-Bis(trimethyltin)-4,8-bis(triisopropylsilylethynyl)-benzo[1,2-b:4,5-b']di-thiphene (TIPSBDT-Tin). Under the protection of N_2, to a suspension of compound **2** (2 g，3.6 mmol) and tetramethylethylenediamine (1.2 mL, 7.56 mmol) in THF (80 mL) was slowly added *n*-BuLi (3.15 mL, 7.56 mmol, 2.4 M) at -78°C. After stirring at low temperature for 1 h, trimethyltinchloride (10.8 mmol) was added in one portion. The reaction mixture was allowed to warm to room temperature overnight. The reaction mixture was quenched with water. The residue was extracted with chloroform and washed with brine and water. The combined organic layer was dried over $MgSO_4$ and concentrated in vaccuo. The crude compound was recrystallized with isopropyl alcohol to give the *title* compound as a pale yellow solid (1.9 g, 88%). ^{1}H NMR (500 MHz, $CDCl_3$, ppm) δ: 7.66 (s, 2H), 1.23 (m, 42H), 0.47 (s, 18H).

Synthesis of polymers. The polymers PBDT-TTz, PTIPSBDT-DTBO and PBDT-DTBTQx were synthesized by Stille coupling reaction. The general synthetic procedure was described as follows. TIPSBDT-Tin (0.2 mmol) and TTz (or DTBO and DTBTQx) based dibromo monomer (0.2 mmol) were dissolved in a mixed solvent of anhydrous toluene (5 mL) and DMF (1 mL). The mixture solution was purged with nitrogen for 15 min before $Pd(PPh_3)_4$ (12 mg, 0.01 mmol) was added. After degassed for another 15 min, the mixture solution was stirred at 105°C for 48 h. The reaction mixture was added dropwise to methanol (200 mL). The collected solid was then subjected to Soxhlet extraction with methanol and acetone. Subsequently, the residue was washed with chloroform and concentrated using rotary evaporator. By re-precipitating from methanol and drying in vaccuo, the *title* polymer was obtained for characterization. **PTIPSBDT-TTz:** a purple solid (240 mg, 82%); ^{1}H NMR (500 MHz, $CDCl_3$, ppm) δ: 7.61-7.60 (br, 2H), 7.55-7.53 (br, 2H), 4.4-4.1 (br, 4H), 1.8-1.0 (br, 82H), 0.8-0.6 (br, 42H); GPC: M_n=12.5 kDa, M_w/M_n (PDI)=1.38; Elemental anal. cald. for $[(C_{48}H_{128}N_2O_2S_6Si_2)_n]$: C 56.85, H 12.72, N 2.76, S 18.97; Found: C 56.79, H 12.70, N 2.71, S 18.96. **PTIPSBDT-DTBO:** a blue solid (200 mg, 70%); ^{1}H NMR (500 MHz, $CDCl_3$, ppm) δ: 8.5-8.3 (br, 4H), 7.9-7.8 (br, 2H), 4.1-4.0 (br, 4H), 1.7-0.88 (br, 72H); GPC: M_n=13.2 kDa, PDI=1.40; Elemental anal. cald. for $[(C_{62}H_{82}N_2O_3S_4Si_2)_n]$: C 68.33, H 7.77, N 2.57, S 11.77; Found: C 68.29, H 7.76, N 2.55, S 11.75. **PTIPSBDT-DTQ:** a black solid (240 mg, 88%); ^{1}H NMR (500 MHz, $CDCl_3$, ppm) δ: 8.96-8.95 (2H), 7.85-7.82 (2H), 7.61-7.59 (2H), 7.33-7.32 (2H), 6.92-6.91 (2H), 3.9-3.8 (8H), 1.5-0.88 (138H); GPC: M_n=15.2 kDa, PDI=1.48; Elemental anal. cald. for $[(C_{108}H_{154}N_4O_4S_5Si_2)_n]$: C 72.43, H 8.78, N 3.13, S 8.95; Found: C 72.40, H 8.86, N 3.10, S 8.96.

4.2. Characterization

^{1}H NMR and ^{13}C NMR spectra were characterized on Bruker AVANCE 500-MHz (Bio-Spin Corporation, Europe) spectrometer with $CDCl_3$ as solvent and tetramethylsilane (TMS) as internal standard. Gel permeation chromatography (GPC) analysis was measured with on a Waters 717-2410 instrument with polystyrene as the standard and THF as eluent (flow rate 1.0 mL/min). Ultraviolet-visible (UV-vis) absorption spectra were recorded on a UV-vis instrument Evolution 220. Thermogravimetric analysis (TGA) analyses were conducted with a TA instrument TGA/SDTA851e with heating rate of 20°C min^{-1} under nitrogen gas flow. The electrochemical cyclic voltammetry was conducted on an electrochemical workstation (CHI660D, Chenhua Shanghai) with Pt plate as working electrode, Pt slice as counter electrode, and saturated calomel electrode (SCE) as reference electrode in tetrabutylammonium hexafluorophosphate (Bu_4NPF_6, 0.1 M) acetonitrile solutions at a scan rate of 50 mV/s. Atomic force microscopy (AFM) was recorded on a Dimension Icon AFM in tapping mode.

4.3. Fabrication and characterization of polymer solar cells

The BHJ solar cells were prepared with a device structure of

ITO/PEDOT:PSS (40 nm)/active layer (~90 nm)/with or w/o PFN (5 nm)/Al (100 nm). The ITO glass substrates were unltrasonicated sequentially in deionized water, acetone, toluene and isopropanol. Immediately prior to device fabrication, the substrates were treated by oxygen plasma for 4 min. Firstly, poly(3,4-ethylenedioxythiophene)/poly(styrene sulfonate) (PEDOT/PSS, H. C. Starck) thin film (40 nm) was spin-coated and then baked at 50°C for 15 min. Secondly, the polymer:$PC_{71}BM$ (1:1, 1:2, weight ratio) blend active layer, with a nominal thickness of ~90 nm, was spin-coated on top of the PEDOT/PSS from a solvent of chloroform (CF) or mixed solvent of chlorobenzene/1,8-diiodoctane (DIO) (95:5 vol%) (10 mg/mL) at 1000 rpm for 2 min. Thirdly, for the insertion of PFN, the PFN material was dissolved in methanol under the presence of small amount of acetic acid and its solution was spin-coated on the top of the obtained active layer to form a thin interlayer of 5 nm. For methanol treatment, after drying of the active layer under vacuum, methanol solvent exposure was carried out by spin-coating methanol on the top of active layers at 2000 rpm for 30 s. For treatment of THF annealing, the devices before PFN/Al deposition were transferred to a glass Petri dish containing THF solvent and covered with a glass cap. After solvent annealing, the samples were dried overnight (>12 h) at room temperature in a N_2-filled glovebox. Al electrode (100 nm) was evaporated through a shadow mask to define the active area of the devices (2×8 mm^2). The current-voltage (*J-V*) characteristics and PCE were measured with a Keithley 2400 sourcemeter under 1 sun, AM 1.5G spectrum from a solar simulator (Oriel model 91192) at room temperature in a nitrogen filled glovebox. Solar simulator illumination intensity was determined using a monocrystal silicon reference cell (HamamatsuS1133, with KG-5 visible color filter) calibrated by the National Renewable Energy Laboratory (NREL).

Acknowledgements

This work is supported by the National Natural Science Foundation of China (Grant No. 21074055), Program for New Century Excellent Talents in University (NCET-12-0633), The Jiangsu Province Natural Science Fund for Distinguished Young Scholars (BK20130032), Doctoral Fund of Ministry of Education of China (No. 20103219120008), and the Fundamental Research Funds for the Central Universities (30920130111006).

Notes and references

[a] *Key Laboratory of Soft Chemistry and Functional Materials (Ministry of Education of China), Nanjing University of Science and Technology, Nanjing 210094, China. Fax: +86 25 8431 7311; Tel: +86 25 8431 7311; E-mail: whtang@mail.njust.edu.cn*

[b] *Institute of Polymer Optoelectronic Materials and Devices, State Key Laboratory of Luminescent Materials and Devices, South China University of Technology, Guangzhou, 510640, China. E-mail: hbwu@scut.edu.cn*

[c] *Key Laboratory of Luminescence and Optical Information (Ministry of Education), Beijing Jiaotong University, Beijing 100044, China*

[d] *Key Laboratory of Preparation and Applications of Environmental Friendly Materials (Ministry of Education of China), Jilin Normal University, Siping 136000, China*

† Electronic Supplementary Information (ESI) available: Synthesis of accepting monomers, NMR spectra and devices data for cells processed using CF. See DOI: 10.1039/b000000x/

‡ These authors contributed equally.

1 H. Chen, J. Hou, S. Zhang, Y. Liang, G. Yang, Y. Yang, L. Yu, Y. Wu and G. Li, *Nat. Photon*., 2009, **3**, 649.
2 L. Bian, E. Zhu, J. Tang, W. Tang and F. Zhang, *Prog. Polym. Sci.,* 2012, **37**, 1292.
3 S. Günes, H. Neugebauer and N. S. Sariciftci, *Chem. Rev.,* 2007, **107**, 1324.
4 G. Dennler, M. C. Scharbe and C. J. Brabec, *Adv. Mater.,* 2009, **21**, 1323.
5 P. M. Beaujuge and J. M. J. Fréchet, *J. Am. Chem. Soc.,* 2011, **133**, 20009.
6 (a) W. Tang, L. Ke, L. Tan, T. Lin, T. Kietzke and Z.-K. Chen, *Macromolecules,* 2007, **40**, 6164; (b) E. Zhu, J. Hai, Z. Wang, B. Ni, Y. Jiang, L. Bian, F. Zhang and W. Tang, *J. Phys. Chem. C,* 2013, **117**, 24700.
7 L. Dou, J. Gao, E. Richard, J. You, C.-C. Chen, K. C. Cha, Y. He, G. Li and Y. Yang, *J. Am. Chem. Soc.,* 2012, **134**, 10071.
8 Y. Li, Z. Pan, L. Miao, Y. Xing, C. Lia, and Y. Chen, *Polym. Chem.,* 2014, **5**, 330.
9 Z. He, C. Zhong, X. Huang, W.-Y. Wong, H. Wu, L. Chen, S. Su and Y. Cao, *Adv. Mater.,* 2011, **23**, 4636.
10 C.E. Small, S. Chen, J. Subbiah, C.M. Amb, S.-W. Tsang, T.-H. Lai, J. R. Reynold and F. So, *Nat. Photon.*, 2012, **6**, 115.
11 X. Li, W.C.H. Choy, L. Huo, F. Xie, W. E. I. Sha, B. Ding, X. Guo, Y. Li, J. Hou, J. You and Y. Yang, *Adv. Mater.,* 2012, **24**, 3046.
12 Z. He, C. Zhong, S. Su, X. Miao, H. Wu and Y. Cao, *Nat. Photon.,* 2012, **6**, 593.
13 F. Huang, K.-S. Chen, H.-L. Yip, S. K. Hau, O. Acton, Y. Zhang, J. Luo, A. K.-Y. Jen, *J. Am. Chem. Soc.,* 2009, **131**, 13886.
14 P. Shen, H. Bin, L. Xiao and Y. Li, *Macromolecules,* 2013, **46**, 9575.
15 L. Huo, S. Zhang, X. Guo, F. Xu, Y. Li, J. Hou, *Angew. Chem. Int. Ed.,* 2011, **50**, 9697.
16 M. Zhang, Y. Gu, X. Guo, F. Liu, S. Zhang, L. Huo, T. P. Russell and J. Hou *Adv. Mater.,* 2013, **25**, 4944.
17 T.-Y. Chu, J. Lu, Y. Zhang, J.-R. Pouliot, J. Zhou, A. Najari, M. Leclerc, Y. Tao, *Adv. Funct. Mater.,* 2012, **22**, 2345.
18 D. Gendron, P.-O. Morin, P. Berrouard, N. Allard, C. N. Garon, Y. Tao and M. Leclerc, *Macromolecules,* 2011, **44**, 7188.
19 X. Guo, N. Zhou, S. J. Lou, J. W. Hennek, R. P. Ortiz, M. R. Butler, P.-L. T. Boudreault, J. Strzalka, P.-O. Morin, M. Leclerc, J.T. López Navarrete, M. A. Ratner, L. X. Chen and R. P. H. Chang, A. Facchetti and T. J. Marks, *J. Am. Chem. Soc.,* 2012, **134**, 18427.
20 E. Zhu, B. Ni, B. Zhao, J. Hai, L. Bian, H. Wu and W. Tang, *Macromol. Chem. Phys.,* 2014, **215**, 227.
21 P. Shen, H. Bin, Y. Zhang and Y. Li, *Polym. Chem.,* 2014, **5**, 567.
22 Y. Wang, Y. Liu, S. Chen, R. Peng and Z. Ge, *Chem. Mater.,* 2013, **25**, 3196.
23 Y. Dong, X. Hu, C. Duan, P. Liu, S. Liu, L. Lan, D. Chen, L. Ying, S. Su, X. Gong, F. Huang and Y. Cao, *Adv. Mater.,* 2013, **25**, 3683.
24 T. Yang, M. Wang, C. Duan, X. Hu, L. Huang, J. Peng, F. Huang and X. Gong, *Energy. Environ. Sci.* 2012, **5**, 8208.
25 M. Wang, X. Hu, P. Liu, F. Huang and Y. Cao, *J. Am. Chem. Soc.,* 2011, **133**, 9638.
26 J. Min, Z. Zhang, S. Zhang, X. Li, X. Gong, F. Huang and Y. Cao, *Chem. Mater.,* 2012, **24**, 3247.
27 K. Li, Z. Li, K. Feng, X. Xu, L. Wang and Q. Peng, *J. Am. Chem. Soc.,* 2013, **135**,13549.
28 E. Zhu, G. Ge, J. Shu, M. Yi, L. Bian, J. Hai, J. Yu, Y. Liu, J. Zhou and W. Tang, *J. Mater. Chem. A*, 2014, **2**, 13580.
29 Q. Shi, H. Fan, Y. Liu, W. Hu, Y. Li and X. Zhan, *Macromolecules,* 2011, **44,** 9173.
30 J.-H. Kim, C. E. Song, H. U. Kim, A. C. Grimsdale, S-J. Moon, W. S. Shin, S. K. Choi, D.-H. Hwang, *Chem. Mater.,* 2013, **25**, 2722.
31 S. Subramaniyan, H. Xin, F. S. Kim, N. M. Murari, B. A. E. Courtright and S. A. Jenekhe, *Macromolecules,* 2014, dx.doi.org/10.1021/ma500250j.
32 J. Hai, W. Yu, E. Zhu, L. Bian, J. Zhang and W. Tang, *Thin Solid Films,* 2014, **562**, 75.
33 J. H. Park, J. S. Kim, J. H. Lee, W. H. Lee and K. Cho. *J. Phys. Chem. C,* 2009, **113**, 17579.
34 G. Li, Y. Yao, H. Yang, V. Shrotriya, G. Yang and Y. Yang, *Adv. Funct. Mater.,* 2007, **17**, 1636.
35 I. Marina, K. Yoshiko, S. Akinori, I. Yuta, O. Hideo, I. Shinzaburo and S. Shu, *J. Phys. Chem. C*, 2013, **117**, 26859.

36 M. C. Scharber, D. Mu; M. Koppe, P. Denk, C. Waldauf, A. J. Heeger and C. J. Brabec, *Adv. Mater.,* 2006, **18**, 789.